Available online at www.sciencedirect.com
ScienceDirect
International Journal of Heat and Mass Transfer 51 (2008) 1264–1280
International Journal of HEAT and MASS TRANSFER
www.elsevier.com/locate/ijhmt

Thermodynamic and kinetic study of transport and reaction phenomena in gallium nitride epitaxy growth

D. Cai [a], W.J. Mecouch [b], L.L. Zheng [a,*], H. Zhang [a], Z. Sitar [b]

[a] Department of Mechanical Engineering, Stony Brook University, Stony Brook, United States
[b] Department of Materials Science and Engineering, North Carolina State University, United States

Received 20 September 2006; received in revised form 3 November 2007
Available online 18 January 2008

Abstract

An iodine vapor phase epitaxy (IVPE) system has been designed and built to grow high quality thick gallium nitride film at the growth rate up to 80 μm/h with the deposition temperature of 1050 °C and the pressure of 200 torr. Numerical and experimental studies have been performed to investigate heat and mass transport and reaction phenomena in a vertical reactor. Geometrical parameters and operating conditions are optimized to achieve high and uniform GaN deposition rate. Gas phase and surface reactions in the growth chamber have been analyzed thermodynamically and kinetically, and primary transport species and important reactions are identified. The rate expressions for different surface reactions are determined and their contributions to the GaN deposition rate are studied for different V/III ratios. The sticking probability of the main reactants and adsorption activation energy are calculated.

Keywords: Computer simulation; Heat and mass transfer; Chemical reaction; Thermodynamics; Kinetics; Semiconductor; Gallium Nitride

1. Introduction

GaN is a wide-bandgap semiconductor with broad applications in blue-green opto-electronic devices and high-temperature transistors [1,2]. Due to unavailable of GaN substrate, GaN thin films have been mainly deposited onto a foreign substrate made by sapphire, silicon carbide, $LiGaO_2$ or $LiAlO_2$ [3]. The use of a foreign substrate, however, will introduce large stresses and defects caused by lattice and thermal expansion coefficient mismatches [4]. To overcome this problem, significant efforts have been directed to produce a thick GaN film (100–200 μm) on a foreign substrate. The deposited thick film is then separated from the original substrate using laser or other means to obtain a self-standing GaN substrate for subsequent growth of epilayers and quantum structures. This technology, however, suffers from low growth rate, low quality and high defect density. This paper will focus on the growth rate and film uniformity during iodine vapor phase epitaxy.

Hydride vapor phase epitaxy (HVPE) method has been widely used to produce GaN thick films with the growth rate up to 50 μm/h and acceptable thickness uniformity [5,6]. In the HVPE system, GaN is grown from reactions of NH_3/GaCl or NH_3/$GaCl_3$. However, the use of HCl gas to obtain $GaCl_x$ in the reactor creates contamination due to corrosion of HCl. To prevent this problem, Bliss and coworkers [7,8] developed an iodine vapor phase epitaxy (IVPE) growth system in which solid iodine vaporizes and reacts with gallium source to form GaI_x. Using a horizontal IVPE system, GaN films at the growth rate on the order of 10 μm/h were demonstrated with a low level of yellow luminescence in the produced GaN films, indicating the beneficial effect of reduced contamination in the process gases. To increase the growth rate and improve the deposition quality, a vertical up-flow IVPE system has been designed and built at North Carolina State University to grow GaN thick films on square SiC substrates. Experiments show that the properties of the deposited GaN films are largely affected by

* Corresponding author. Tel.: +1 631 632 8346; fax: +1 631 632 8544.
E-mail address: lili.zheng@stonybrook.edu (L.L. Zheng).

0017-9310/$ - see front matter © 2007 Elsevier Ltd. All rights reserved.
doi:10.1016/j.ijheatmasstransfer.2007.12.004

Nomenclature

A_p	pre-exponential coefficient of reaction constant (s^{-1} for a first order reaction)
C	species concentration (mol/m^3)
c_P	specific heat of gas (m^2 s^{-2} K^{-1})
d	diameter (m)
D	binary diffusion coefficient (m^2/s)
D_a^g	gas phase Damkohler number ($r_0^g L_c/V_0$)
D_a^s	surface Damkohler number ($r_0^s L_c/V_0$)
E_a	activation energy (J/mol)
F_i	surface incident of species i (kmol m^{-2} s^{-1})
$\vec{g}$	acceleration due to gravity (m/s^2)
Gr	Grashof number $g\rho_0^2 L_c^3 (T_w - T_{in})/(\mu_0^2 T_0)$
h	enthalpy (J/mol)
I	radiation heat flux (w/m^2)
I_b	intensity of the black body (w/m^2)
k	thermal conductivity (J m^{-1} s^{-1} K^{-1})
k_r	reaction coefficient (m^3/mol s)
L	exposure length for diffusion (m)
L_c	characteristic dimension (m)
$\dot{m}$	species mass reduction rate (kg/s)
m	exponent on pressure dependency of reaction constants
n	temperature exponent of reaction constants
Nu	Nusselt number (h d/k)
P	pressure (kg m^{-1} s^{-2})
Pe_T	thermal Peclet number ($\rho_0 c_{P0} V_0 L_c/k_0$)
Pe_M	mass Peclet number ($V_0 L_c/D_0$)
Pr	Prandtl number ($\mu_0 c_{P0}/k_0$)
P_{ref}	referent reactor pressure (kg m^{-1} s^{-2})
Q	flow rate (m^3/s)
r	radius (m)
r_0^g	gas phase reaction constant (mol m^{-3} s^{-1} for a first order reaction)
r_0^s	surface reaction constant (mol m^{-2} s^{-1} for a first order reaction)
R	gas constant (J kmol^{-1} K^{-1})
Re	Reynolds number ($\rho_0 V_0 L_c/\mu_0$)
Re_D	Reynolds number ($\rho_0 V_0 d_0/\mu_0$)
R_i	surface adsorption rate of species i (kmol m^{-2} s^{-1})
S_i	sticking probability of species i
S_h	heat source due to reaction (w m^{-2} s^{-1})
T	temperature (K)
T_{amb}	ambient temperature (K)
T_{in}	gas temperature at inlets (K)
T_m	longitudinal average gas temperature (K)
T_w	wall temperature (K)
U_{av}	averaged velocity (m/s)
$\underrightarrow{V}$	vacant surface site of species adsorption
$\vec{V}$	gas velocity vector (m/s)
W_i	molecular weight of species i (kg/kmol)
$\dot{w}_i^g$	gas phase reaction rate (mol/m^3 s)
$\dot{w}_i^s$	surface reaction rate (mol/m^2 s)
X	axial distance (m)
Y_i	mass fraction of species i

Greek symbols

α	concentration exponents of species A for a second order reaction
α_T	thermal expansion coefficient ($k/\rho/C_p$)
β	concentration exponents of species B for a second order reaction
ρ	density (kg/m^3)
μ	dynamic viscosity (kg m^{-1} s^{-1})
ε	radiative emissivity
τ	viscous stress tensor
δ	deposition coefficient
Ω	direction of the radiation beam
κ	radiative absorption coefficient
σ	scattering coefficient
θ	silica nozzle angle (°)
θ^s	surface coverage of species i

process conditions such as reactor pressure, furnace temperature, species concentration and flow rate.

Numerical simulation has become a vital tool to reveal process characteristics of GaN growth. It has been used to simulate metalorganic chemical vapor deposition (MOCVD) and HVPE GaN growth [9–13] and study the effects of growth parameters on uniformity and material properties of the deposited GaN films. No simulation has yet been published in the literature on IVPE GaN growth. Understanding of the heat and mass transport in such reactor and the GaN growth mechanism on a SiC substrate is therefore poor. This paper will investigate heat and mass transport and reaction phenomena in the vertical reactor built in North Carolina State University (NCSU) using an integrated modeling and experimental approach. Geometrical parameters and operating conditions are optimized to achieve high and uniform GaN deposition rate. Gas phase and surface reactions in the growth chamber are analyzed thermodynamically and kinetically, so as to identify the primary transport species and important reactions. The rate expressions for different surface reactions are determined and their contributions to the GaN deposition rate are studied for different V/III ratios. The sticking probability of the main reactants and adsorption activation energy are calculated.

2. Experimental setup

Schematic of the proposed vertical reactor is presented in Fig. 1a. Iodine vapor is used to transport Ga from source to substrate to grow GaN. Ammonia gas is introduced to provide the nitrogen source for GaN growth.

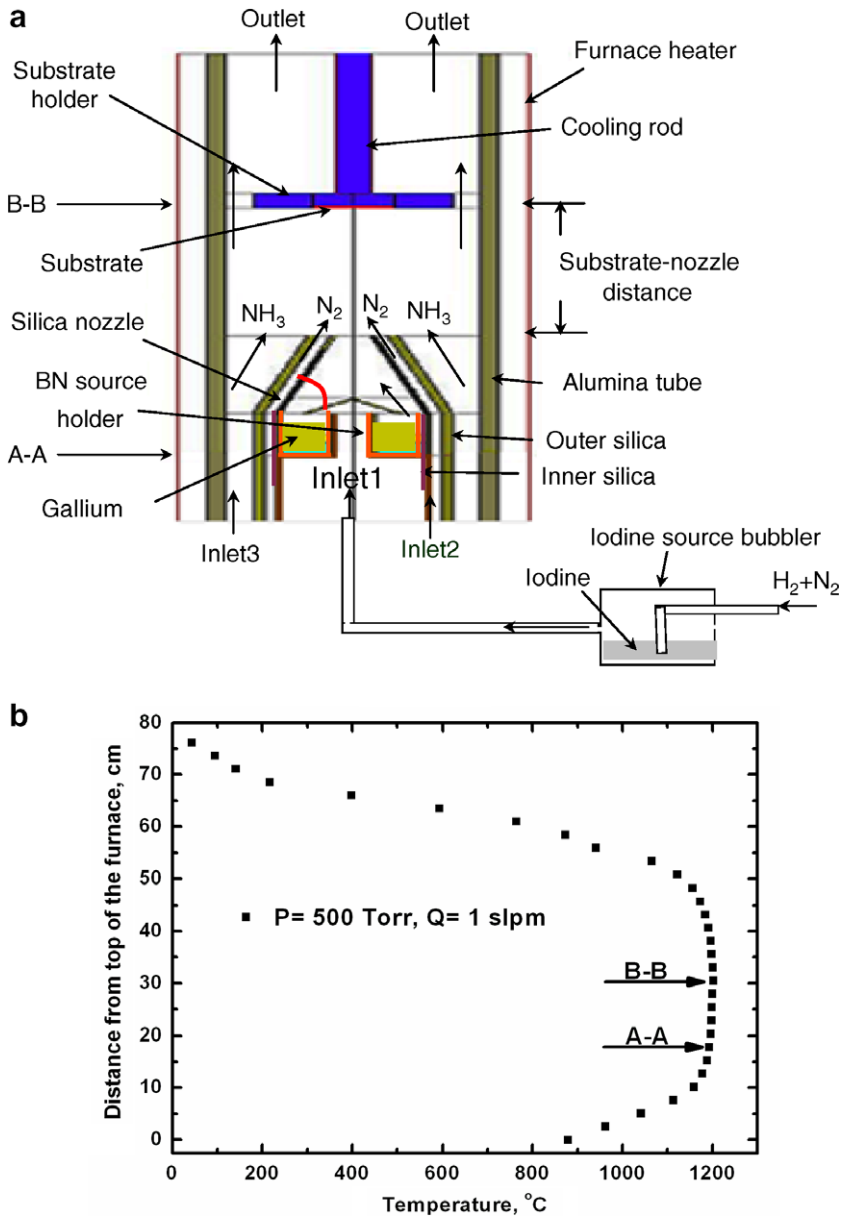

Fig. 1. (a) Schematic of the reaction chamber and (b) measured temperature profile from top to bottom along the furnace wall.

The reactor consists of four concentric tubes: furnace tube, reactor tube, outer silica tube and inner silica tube. Iodine is carried by nitrogen and hydrogen flowing upwards through the inner silica. At the top of the inner silica tube is the gallium source within a BN holder. The iodine reacts with Ga melt to form GaI_x. A silica nozzle is placed above the gallium source to enhance Ga replacement. The gas flowing out of the silica nozzle is, therefore, a mixture of nitrogen, iodine, hydrogen, GaI_x and gallium. Between the inner and outer silica tubes, nitrogen is flowed to shield the Ga from the ammonia in the gas phase and enhance reactions on the substrate. Finally, the ammonia and nitrogen mixture flows through the space between the reactor tube and the outer silica tube. The entire system is heated by a resistant heater. The temperature calibration of the furnace has been conducted under reactor pressure of 500 torr and nitrogen flow rate of 1 SLM. Fig. 1b shows the temperature profile measured by thermocouple along the furnace wall. By setting the growth temperature at 1200 °C, the uniform temperature zone achieved is about 38.1 cm. The gallium source (position A-A) and the substrate (position B-B) are both positioned in the uniform temperature zone. The gallium source is positioned close to the bottom of the zone so as to ensure the entire growth area is located in the uniform temperature zone.

3. Mathematical model for numerical simulation

3.1. Governing equations

The following assumptions are made in this paper: (a) The system is axi-symmetric; (b) The gas mixture is

continuum; (c) The gases obey the ideal-gas law; (d) The gas flow is laminar; (e) The gas mixture in the reactor is transparent for thermal radiation; and (f) Viscous dissipation of the gas mixture is neglected. Based on the above assumptions, the governing equations of vapor phase deposition can be described as follows [14–16]:

Continuity equation:

$$\frac{\partial \rho}{\partial t} + \nabla \cdot (\rho \vec{V}) = 0; \tag{1}$$

Momentum conservation:

$$\frac{\partial}{\partial t}(\rho \vec{V}) + \nabla \cdot (\rho \vec{V}\,\vec{V}) = -\nabla p + \nabla \cdot \tau + \rho \vec{g}; \tag{2}$$

Energy conservation:

$$\frac{\partial}{\partial t}(\rho h) + \nabla \cdot (\rho \vec{V} h) = \nabla \cdot (k \nabla T) + S_{\mathrm{h}}; \tag{3}$$

Species conservation:

$$\frac{\partial}{\partial t}(\rho Y_i) + \nabla \cdot (\rho \vec{V} Y_i) = \nabla \cdot (\rho D \nabla Y_i) + \dot{\omega}_i^{\mathrm{g}}; \tag{4}$$

where ρ is the density, $\vec{g}$ is the gravitational acceleration vector, $\vec{V}$ is the gas velocity, p is the pressure, τ is the viscous stress tensor, h is the enthalpy, T is the temperature, k is the thermal conductivity, S_{h} is the additional source due to reactions and radiation, D is the binary diffusion coefficient of reactants in carrier gases, $\dot{w}_i^{\mathrm{g}}$ is the gas phase reaction rate of species i, and Y_i is the mass fraction of species i.

The integro-differential radiative heat transfer equation used to calculate the energy source from radiation can be described as follows [17]:

$$(\Omega \cdot \nabla) I(r,\Omega) = -(\kappa+\sigma) I(r,\Omega) + \kappa I_{\mathrm{b}}(r) + \frac{\sigma}{4\pi}\int_{\Omega'=4\pi} I(r,\Omega)\Phi(\Omega' \to \Omega)\,\mathrm{d}\Omega, \tag{5}$$

where Ω is the direction of propagation of radiation beam, I is the radiation intensity, κ is the absorption coefficient, σ is the scattering coefficient, I_{b} is the intensity of the black body, and Φ is the phase function of the energy transfer from the incoming Ω' direction to the outgoing direction Ω.

As an additional constraint of the governing equations, the ideal gas law can be described as

$$p = \rho R T \sum_i \frac{Y_i}{W_i}, \tag{6}$$

where W_i is the molecular weight of species i and R is the gas constant.

3.2. Boundary conditions

Boundary conditions are prescribed as follows:

Wall on the graphite heater: $\vec{V} = 0$, $T = 1323$ K, $\varepsilon = 1.0$;
Wall on the substrate holder: $\vec{V} = 0$, $\varepsilon = 0.65$;
Top surface of the gallium source: $\dot{w}_{\mathrm{gallium}} = \dot{w}_1$, $T = 700$ K, $\varepsilon = 0.6$;
Wall on the surface of the substrate: $\vec{V} = 0$, $J_i = M_i \dot{w}_i^{\mathrm{s}}$, $\varepsilon = 0.65$;
Wall on the alumina tube: $\vec{V} = 0$, $\varepsilon = 0.7$;
Wall on the quartz surface: $\vec{V} = 0$, $\varepsilon = 0.14$;
Carrier gas at the inlet (ammonia and nitrogen): $\vec{V} = \vec{V}_1$, $T = 700$ K, $P_{\mathrm{in}} = P_{\mathrm{ref}}$, $Y_{\mathrm{NH_3}} = Y_1$, $Y_{\mathrm{N_2}} = Y_2$, $\varepsilon = 0.15$;
Iodine source at the inlet (I_2, N_2 and H_2): $\vec{V} = \vec{V}_2$, $T = 700$ K, $P_{\mathrm{in}} = P_{\mathrm{ref}}$, $Y_{\mathrm{I_2}} = Y_3$, $Y_{\mathrm{N_2}} = Y_4$, $Y_{\mathrm{H_2}} = Y_5$, $\varepsilon = 0.15$;
Shield gas at the inlet (nitrogen): $\vec{V} = \vec{V}_3$, $T = 700$ K, $P_{\mathrm{in}} = P_{\mathrm{ref}}$, $Y_{\mathrm{N_2}} = Y_6$, $\varepsilon = 0.15$;
Outlet: $T = 300$ K, $P_{\mathrm{out}} = P_{\mathrm{ref}}$, $\varepsilon = 1.0$.

Non-slip boundary condition, $\vec{V} = 0$, is applied for all the walls. Since the growth cell simulated is positioned in the uniform temperature zone, a constant temperature, $T = 1323$ K, is assigned on the surface of the furnace wall with radiative emissivity, ε, of 1. The experimentally measured weight losses of iodine and Ga sources are converted to mass flow rates in the model and used as inlet gas flow rates. The surface reaction rate, $\dot{w}_i^{\mathrm{s}}$, is converted to the mass flux, J_i, and treated as the boundary conditions on the substrate surface. The pressure condition at outlet will only be used when there is back flow.

4. Control parameters

The order-of-magnitude analysis is presented here to provide fundamental understanding of heat and mass transfer in the GaN iodine growth system. Important dimensionless groups, definitions and calculated values in the growth system are listed in Table 1. L_{c} is the characteristic length, defined as the diameter of the alumina reactor, V_0 is the characteristic velocity, defined as the inlet process gas velocity, and Y_i^{in} is the characteristic mass fraction of species i, defined as the inlet mass fraction of species i. Noted that subscript 0 represents the value at the average temperature of $T_{\mathrm{av}} = (T_{\mathrm{w}} + T_{\mathrm{in}})/2$, where T_{w} is the temperature achieved on the furnace heater, which is about 1323 K, and T_{in} is the mean temperature of the inlet gases, which is about 700 K.

According to the calculated values in Table 1, gas flow is mainly laminar in the reactor, and heat and mass transfer due to convection is more important than conduction/diffusion. The ratio of the Grashof number, Gr, to Reynolds

Table 1
Important dimensionless groups in the IVPE reactor

Dimensionless group	Definition	Value
Reynolds (Re)	$\rho_0 V_0 L_0/\mu_0$	37.7
Grashof (Gr)	$g\beta_0\rho_0^2 L_{\mathrm{c}}^3(T_w - T_{\mathrm{in}})/\mu_0^2$	940.0
Prandtl (Pr)	$\mu_0 C_{\mathrm{P}0} K_0$	0.64
Schmidt (Sc)	$\mu_0/\rho_0 D_0$	0.73
Thermal Peclet (Pe_{T})	$Re \cdot Pr$	24.2
Mass Peclet (Pe_{M})	$Re \cdot Sc$	27.4
Gas-phase Damkohler (Da^{g})	$r_0^{\mathrm{g}} L_{\mathrm{c}}/V_0$	/
Surface Damkohler (Da^{s})	$r_0^{S} L_{\mathrm{c}}/V_0$	/

number square, Re^2, is used to examine whether heat transfer is mainly controlled by natural or forced convection. $Gr/Re^2 = 0.66$ is obtained for the system discussed here, indicating that natural and forced convection heat transfer are equally important.

5. Gas phase and surface reactions

5.1. Gas phase reactions

In the GaN epitaxy growth system, the carrier gas mixture of N_2 and H_2 enters I_2 source bubbler, where I_2 ($T_{melting} = 385.9$ K at 1 atm) is heated by a jacket heater. I_2 is vaporized and carried away by the carrier gas. I_2 may react with H_2 to form HI. The gas mixture of N_2, H_2, I_2 and HI will, therefore, flow over the gallium source. Both I_2 and HI may react with Ga to form GaI_x, with $x = 1$ or 3. On the substrate surface, NH_3 will be adsorbed and cracked to form the activated nitrogen atoms that will react with GaI_x to form GaN on the substrate [18]. It is important to control the concentration of NH_3 and GaI_x on the substrate surface. Gas species reaching the substrate include NH_3, HI, H_2, N_2, GaI, GaI_3, I_2 and Ga. The detailed gas pathway is shown in Fig. 1a.

Before ammonia reaches the substrate, it may decompose to nitrogen and hydrogen gases due to the high-temperature environment in the growth reactor. The amount of ammonia reaching the substrate is therefore reduced. The global ammonia gas phase decomposition can be expressed as follows:

$$NH_3(g) \iff 1/2N_2(g) + 3/2H_2(g). \quad (R1)$$

This is a mildly endothermic process ($\Delta H = 46$ kJ/mol). Thermodynamically, almost all the NH_3 is decomposed into N_2 and H_2 at the temperature higher than 300 °C. In the experiments, the decomposition rate of NH_3 is slow and strongly depends on the growth conditions and furnace geometry. This reaction may, in fact, be far from achieving the equilibrium state.

The Damkohler number has been calculated for ammonia gas phase decomposition to determine the importance of this reaction under the current operating conditions. The fluid flow resident time can be estimated as $t_F = L_F/U_{av}$. L_F is the distance between the gas inlet and the substrate, which is about 0.16 m. The averaged velocity is about 0.67 m/s with a typical flow rate of 3.0 SLM under the pressure of 200 torr and the furnace wall temperature of 1323 K. The resident time can then be calculated as 0.24 s. The detailed mechanism of NH_3 homogeneous pyrolysis can be found in [19]. The controlling step of the reactions is found to be:

$$NH_3 + M \iff NH_2 + H + M, \quad (R2)$$

where M is the third party molecular that serves as a catalyst. Reaction (R2) is a second order reaction with the reaction coefficient $k_r = A_p \mathrm{Exp}(-E_a/RT)$ and a reaction rate $\dot{w}_g = k_r[NH_3][M]$, where the pre-exponential coefficient, A_p, is 2.2×10^{10}, and the reaction activation energy, E_a, is 3.93×10^5 J/mol. The value of k_r is calculated as 2.55×10^{-5} m^3/mol s. The third party molecular concentration is about 1.17 mol/m^3 when the molar ratio of NH_3 and N_2 in the reactor is assumed to be 1. The reaction constant is calculated as $r_0^g = k_r \cdot [M] = 2.98 \times 10^{-5}$ s^{-1}. The gas phase Damkohler number for ammonia pyrolysis is about 7.12×10^{-6}, which is much smaller than 1. It is concluded from this analysis that gas phase ammonia decomposition can be neglected under the current operating conditions.

Instead of reaction on the substrate surface, ammonia may also react with GaI_x in the gas phase. To reduce gas phase reactions between NH_3 and GaI_x, the shield gas, N_2, is running between the inner and outer silica nozzle to prevent direct mixing of NH_3 and GaI_x in the area above the silica nozzle (see Fig. 1a), and meanwhile increase the NH_3 and GaI_x concentrations on the substrate surface. The gas phase reactions between NH_3 and GaI_x are expected to be weak. This reaction can be neglected due to the presence of the shield gas and the short reaction time. It is estimated that the resident time for reaction is about 0.09 s based on the substrate-nozzle distance of 0.0635 m and the gas speed of 0.67 m/s.

The gas phase reaction in the iodine source bubbler can be described as follows:

$$1/2H_2(g) + 1/2I_2(g) \iff HI(g). \quad (R3)$$

The initial partial pressures of H_2, I_2, HI, and N_2 are $P^0_{H_2}$, $P^0_{I_2}$, P^0_{HI} and $P^0_{N_2}$, respectively, where the initial partial pressure of HI equals zero. When reaction equilibrium is reached, the equilibrium partial pressures of species can be expressed as $P^e_{H_2}$, $P^e_{I_2}$, P^e_{HI}, and $P^e_{N_2}$. The total pressure inside the bubbler is maintained at 1 atm and it remains unchanged since the reduced partial pressures of H_2 and I_2 equal the produced partial pressure of HI in the reaction R3. The partial pressure of N_2 remains constant during the reaction. Controlled by the mass flow controllers, the initial molar ratio of H_2 and N_2 in the carrier gas is 9%:91%. At the time zero, the follow equations can therefore be obtained:

$$\sum P^0_i = 1 = P^0_{H_2} + P^0_{I_2} + P^0_{N_2} \quad (7)$$

$$\frac{P^0_{H_2}}{P^0_{N_2}} = \frac{9}{91} \quad (8)$$

$$\frac{P^0_{I_2}}{\sum P^0_i} = [I_2] \quad (9)$$

The initial vapor pressure of the iodine over the source surface, $P^0_{I_2}$, can be obtained from Ref. [20]. The equilibrium expression of reaction (R3) can be written as follows:

$$K_3 = \mathrm{Exp}\left(-\frac{\Delta G^0_r}{RT}\right) = \frac{P^e_{HI}}{\sqrt{P^e_{I_2} P^e_{H_2}}}, \quad (10)$$

where K_3 is the reaction equilibrium constant and ΔG^0_r is the Gibbs free energy change, the temperature dependence

of which can be found in Refs. [21,22]. Two additional equations derived from reaction (R3) are

$$P^0_{H_2} - P^e_{H_2} = P^0_{I_2} - P^e_{I_2}, \quad (11)$$

$$P^e_{HI} = 2(P^0_{I_2} - P^e_{I_2}). \quad (12)$$

Given the initial partial pressure of iodine vapor, the equilibrium pressure of each species in reaction (R3) can be solved by combining Eqs. (7)–(12). Fig. 2a shows the equilibrium partial pressures of different species at the inlet of the reactor under different iodine concentrations in the source. The highest iodine vapor pressure achieved in the source bubbler is limited by the temperature of the valve connected to the bubbler. Since gas temperature can not exceed 150 °C for a regular needle valve, the highest I_2 vapor pressure is about 300 torr in the bubbler. It is revealed that when equilibrium for reaction R3 is established before the gas mixture flows over the gallium source, the concentration of HI gas will be around 0.1. When the concentration of I_2 in the source is larger than 0.3, I_2 will be the main species reacting with gallium to form GaI_x.

The gas mixture coming out of the iodine source bubbler enters the reactor through the inner silica tube and reacts with gallium. Instead of reacting with Ga vapor, both I_2 and HI will react mostly with gallium on its liquid surface due to a low gallium vapor pressure of 0.01 torr [23] at the current operating conditions. The reactions between I_2 and Ga can be written as follows:

$$Ga(l) + 1/2I_2(g) \iff GaI(g), \quad (R4)$$

$$Ga(l) + 3/2I_2(g) \iff GaI_3(g), \quad (R5)$$

$$GaI(l) + I_2(g) \iff GaI_3(g), \quad (R6)$$

and the reactions between Ga and HI can be written as follows:

$$Ga(l) + HI(g) \iff GaI(g) + 1/2H_2, \quad (R7)$$

$$Ga(l) + 3HI(g) \iff GaI_3(g) + 3/2H_2(g), \quad (R8)$$

$$GaI(l) + 2HI(g) \iff GaI_3(g) + H_2(g). \quad (R9)$$

At a typical growth temperature of 1050 °C, the calculated reaction equilibrium constants for reactions (R4)–(R6) are 8900, 840,000, and 50, respectively. The equilibrium reaction constants are 3400, 13,000, and 4 for reactions (R7)–(R9), respectively. The formation of GaI_3 in both cases is strongly favored thermodynamically. It is, therefore, assumed that only GaI_3 will be formed at equilibrium. A group of equations similar to the formation of HI can be derived and the equilibrium partial pressures of species above the gallium source can be calculated. Fig. 2b shows the calculated partial pressures on the gallium source. Comparing Fig. 2b with Fig. 2a, it is revealed that the partial pressure of GaI_3 is seen to track with the initial partial pressure of iodine.

The favorability of reactions (R6) and (R9) indicates that any GaI formed will further react either with I_2 or HI to form GaI_3 at the equilibrium conditions. However, thermodynamic calculations only provide an upper limit of what to expect. Given the small surface area of the gallium source (1.1×10^{-4} m^2), and the relatively high velocity of carrier gas over the gallium source (order of 0.1 m/s), it is unlikely that there is sufficient time for equilibrium conditions to be established above the gallium source. The thermodynamic model describing transport of iodine and gallium species has to be compared with the experimental data to evaluate its accuracy.

Fig. 3a shows the measured gallium loss rate compared with the measured iodine loss rate. The data points by symbols of diamond and square correspond to a carrier gas mixture of 9% H_2/91% N_2, and by symbols of triangle and circle correspond to carrier gas of pure hydrogen. The data are measured based on 20-h growth runs. Also the two lines represent iodine transport as GaI ($Ga/I_2 = 2{:}1$) and GaI_3 ($Ga/I_2 = 2/3$), respectively. It is revealed that the measured iodine loss rate falls between the values calculated based on two transport species. This indicates that there is enough iodine loss to account for GaI transport, but not enough iodine is lost to account for GaI_3 transport. It can be concluded that the dominant transport species is GaI, with some GaI_3 formed either on the Ga surface, or through subsequent reaction with the excess iodine species.

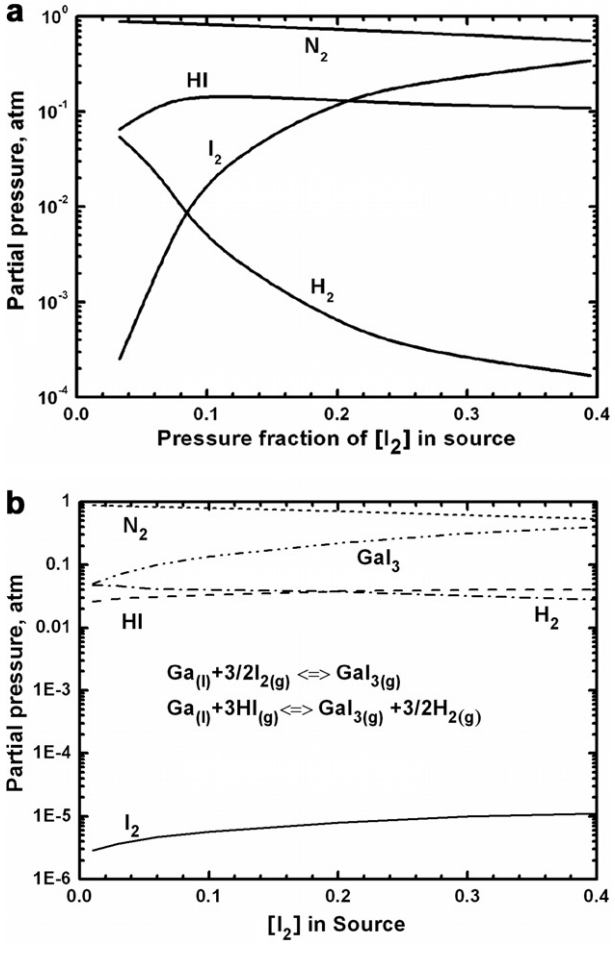

Fig. 2. (a) Equilibrium partial pressures with [I_2] in source, and (b) equilibrium partial pressure above liquid gallium at 1050 °C.

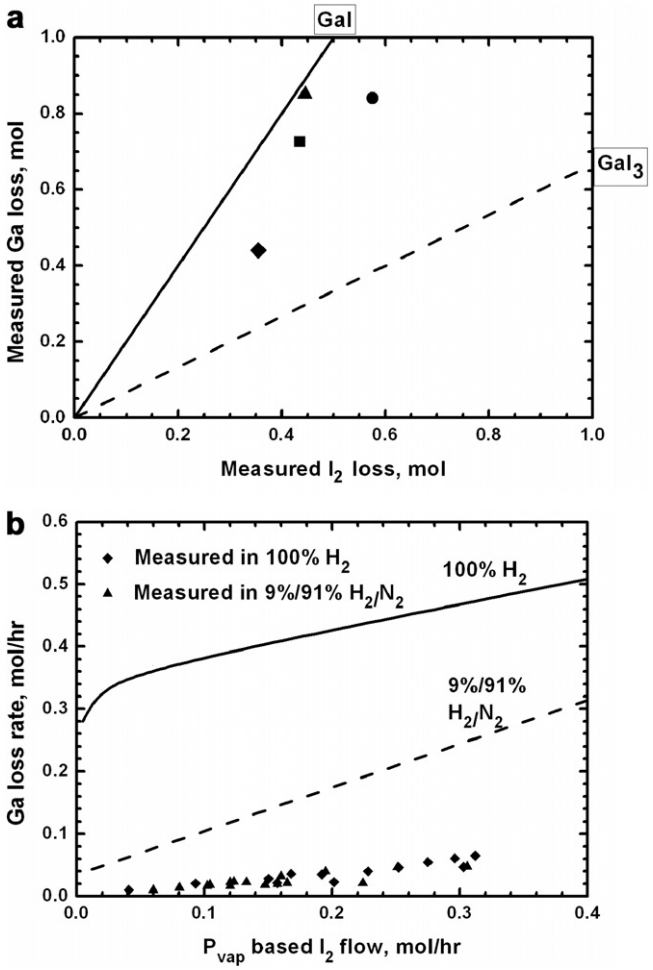

Fig. 3. (a) Measured gallium loss rate versus measured iodine loss rate and (b) Gallium loss rate predicted from GaI_3 based thermodynamic equilibrium as shown in Fig. 2b (lines) and measured during experiment growth runs (diamonds and triangles).

Fig. 3b shows the predicted and measured rates of gallium loss versus the flow rates of I_2. The solid lines represent the results obtained based on thermodynamic equilibrium of GaI_3 reaction, and the diamond and triangle dots represent the measured Ga loss with a pure H_2 carrier gas and a carrier gas mixture of 9% H_2/91% N_2. The experimental values fall well below the equilibrium prediction, and show no difference in measured loss rate of Ga between a carrier gas of pure H_2 and mixture of 9% H_2/91% N_2. This indicates that the source does not operate near the equilibrium as predicted by thermodynamics, and the reaction of HI formation does not significantly increase the transport of iodine. The thermodynamically calculated iodine loss rate is about 10–30 times greater than the measured iodine loss. Even if the assumption is made that iodine is transported from the source at the vapor equilibrium without any reaction to form HI, the calculated iodine flow rate is still 6–9 times higher than the observed loss rate from the iodine source. It is likely that the high flow rate of carrier gas and the crystal shape change in the iodine source as temperature fluctuates both will contribute to the difficulty to achieve equilibrium iodine vapor pressure in the source bubbler.

Based on direct measurement of weight loss from both iodine and gallium sources after each experiment run, Tassev at al. [8] reported that transport species in their reactor was GaI, with a slight excess of I_2. Furthermore, Rolsten [24] reported that GaI can be formed by heating either GaI_3 or the reaction product of gallium and iodine. Based on these results, along with the relatively high flow rate of carrier gas and small volume for reaction, it is assumed that all the measured gallium loss was transported as GaI.

In the numerical model, only reaction R4 will be used to describe the gas phase reaction for GaI_x formation. Measured iodine and gallium mass reduction rates will be converted to the flow rate of I_2 and Ga, respectively. The gas phase reaction rate of reaction (R4) can be described as

$$\dot{\omega}_g = A_p T^n \exp(-E_a/RT)\left(\frac{p}{p_{atm}}\right)^m [A]^\alpha [B]^\beta \text{kmol/m}^3\ \text{s}, \quad (13)$$

where A_p is the pre-exponential constant, n is the temperature exponent, E_a/R is the activation temperature, m is the exponent on pressure dependency, A and B are the molar concentrations of reactants Ga and I_2, and α and β are the concentration exponents of A and B, respectively. $E_a/R = 0$ K and $n = m = 0$ are used in the simulation. The value of A_p is used to determine the reaction rate and it is estimated as 4×10^8 corresponding to more than 95% conversion of experimentally weighted Ga loss to GaI. $\alpha = 1$ and $\beta = 0.5$ are assigned, which correspond to the stoichiometric coefficients of the reactants.

5.2. Surface reactions

The overall surface reaction rate depends on the partial pressures of gas species such as GaI and NH_3, available free sites on the surface, surface concentrations of adsorbed species, surface diffusion coefficients, rate constants of reaction steps, and surface characteristics, etc. Unlike gas phase reaction, predicting reaction paths and rate constants are more difficult for heterogeneous surface reactions since the interaction between gas phase and surface entities are much more complicated than those between gas phase molecules. The semi-empirical approach is, therefore, usually used to simulate the surface mechanisms and kinetics.

Tassav et al. [8] discussed surface reactions from GaI and NH_3. Based on the byproducts detected in their GaN reactor, the one step reaction for the growth of GaN is given as

$$GaI(g) + 2NH_3(g) \rightarrow GaN(s) + NH_4I(g) + H_2(g). \quad (R10)$$

However, NH_4I detected in the cold react zone might be formed from NH_3 and HI with a temperature lower than 800 K since NH_4I decomposes above 800 K [22]. In the growth zone from silica nozzle to the substrate, gas temper-

ature will be close to 1323 K. It is, therefore, unlikely that NH_4I will present. Considering different product gases which are stable at a temperature around 1323 K, the following analogs of element reactions to GaN growth from $GaCl/NH_3$ mixture in a halide vapor phase expitaxy system [18,25] can be expressed as

$$V + NH_3 \iff NH_{3ads}, \quad \text{(R11)}$$

$$NH_{3ads} \iff N + 3/2H_2(g), \quad \text{(R12)}$$

$$N + GaI \iff NGaI, \quad \text{(R13)}$$

$$2NGaI + H_2(g) \iff 2NGa - IH, \quad \text{(R14)}$$

$$NGa - IH \iff NGa + HI(g), \quad \text{(R15)}$$

$$2NGaI + GaI(g) \iff 2NGa - GaI_3, \quad \text{(R16)}$$

$$2NGa - GaI_3 \iff 2NGa + GaI_3, \quad \text{(R17)}$$

where V is the vacant surface site for ammonia adsorption.

Since a very large NH_3 partial pressure is maintained on the substrate in the experiments, reaction (R11) will be close to thermodynamic equilibrium, which means that the NH_{3ads} concentration on the substrate will be close to a constant. The GaN deposition rate is mostly limited by reactions (R13). This is supported by the experimental data whereas GaN growth rate is independent of the NH_3 partial pressure, but strongly depends on the GaI concentration. Since it is difficult to obtain the reaction constant for each elemental step, the simplified overall surface reactions will be used here. Two overall reactions corresponding to above element reactions are obtained as follows:

$$GaI(g) + NH_3(g) \iff GaN(s) + HI(g) + H_2(g), \quad \text{(R18)}$$

$$3GaI(g) + 2NH_3(g) \iff 2GaN(s) + GaI_3(g) + 3H_2(g), \quad \text{(R19)}$$

which represent the most energetically favorable reactions in the iodine vapor growth system. The following reaction might also be energetically favorable since GaI_3 is thermodynamically preferred:

$$GaI_3(g) + NH_3(g) \iff GaN(s) + 3HI(g) \quad \text{(R20)}$$

Reaction (R20) will also be considered in the numerical model, although thermodynamics analysis shows the contribution of reaction (R20) to the GaN deposition rate will be less than 2%.

Fig. 4 shows the free energy of surface reaction for (R18)–(R20) on substrate surface. Since GaI is assumed as the dominant species of gallium transport, reactions (R18) and (R19) are expected to be much more important than reaction (R20). The free energies for reactions (R18)–(R20) are all positive at a typical growth temperature of 1050 °C, which means that their equilibrium reaction constants are smaller than unity, and none of the reactions is spontaneous. A proper effective super-saturation, $\sigma = \ln(P_{GaI}P_{NH_3}/P_{HI}P_{H_2}K_{18})$, can still be achieved by controlling the partial pressures of the reactants on the substrate, which serves as the driving force for the GaN deposition.

Since reactions (R19) and (R20) can be combined to form reaction (R18), reaction (R18) will therefore be used as the overall surface deposition step in our simulation. The surface reaction rate of reaction (R18) is determined by

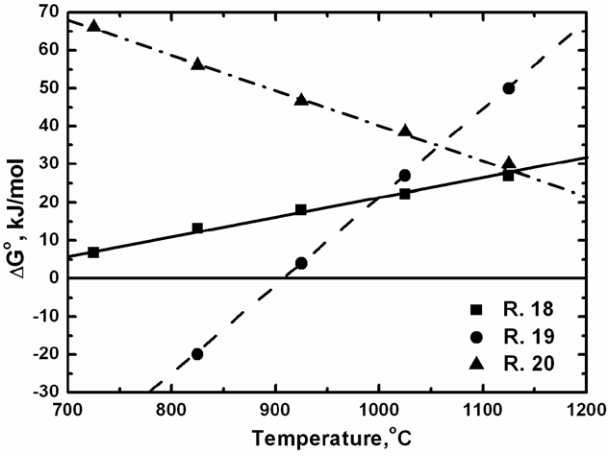

Fig. 4. Free energy of reaction for GaN surface deposition in a vapor growth system.

$$\dot{\omega}_s = \delta A_p T^n \exp(-E_a/RT)\left(\frac{p}{p_{atm}}\right)^m [A]^\alpha [B]^\beta \ \text{kmol/m}^2\ \text{s}, \quad (14)$$

where δ is the deposition coefficient of GaN on the substrate surface. The rate constant, r^s, for reaction (R18) has not been reported in the literature. The activation energy of 1.03×10^5 J/mol is reported in reference to the data from Shintani et al. [26] for the following surface reaction of GaN HVPE growth:

$$GaCl(g) + NH_3(g) \iff GaN(s) + HCl(g) + H_2(g). \quad \text{(R21)}$$

Their data is obtained for the temperature range of 860–1020 °C, which is similar to our growth temperature (1050–1100 °C). The activation energy of 1.03×10^5 J/mol is, therefore, used for reaction (R18). $n = m = 0$ are used in the simulation. $\alpha = x$ and $\beta = 0$ are assigned for concentration coefficients of GaI and NH_3. The value of α is underdetermined since the concentration dependency of GaI should be among 1–3 according to reactions (R18)–(R20). The ammonia concentration dependency is set to zero due to the fact that in the experiment ammonia is always excessive on the substrate surface. By matching the experimental deposition rates with the simulation ones at different NH_3/GaI molar ratios, the value of δA_p and α can be determined by the optimization method.

To determine the importance of reactions (R18)–(R20) for the GaN deposition rate, all three equations are therefore included in the simulations. The respective contribution of the three reactions to the GaN growth rate will be determined based on the assumption that all of the reactions are stoichiometric. No kinetic data for reactions R19,R20 are available in published literatures. Shaw et al. [27] reported that the activation energy of GaAs epitaxial growth is between 6.18×10^4 J/mol and 1.65×10^5

J/mol in the Ga–As–Cl_3 system due to adsorption, reaction, and diffusion at the surface. The activation energy for reaction (R19) is thus chosen as $E_a = 1.13 \times 10^5$ J/mol, which is the medium value of the above energy range. Also for reaction (R19), $n = m = 0$, $\alpha = 3$ and $\beta = 0$, and the value of δA_p is determined by fitting numerical results with the experimental data. $E_a = 1.16 \times 10^5$ J/mol is reported by Dollet et al. [28] for the following surface reaction of AlN expitaxial growth:

$$AlCl_3(g) + NH_3(g) \iff AlN(s) + 3HCl(g). \quad (R22)$$

This activation energy is used for reaction (R20). Also for reaction (R20), $n = m = 0$, $\alpha = 1$ and $\beta = 0$, and $\delta A_p = 0.36$ reported by Cai et al. [29] for reaction (R22) of AlN expitaxial growth with the temperature of 1050 °C and pressure of 760 torr. Finally the GaN deposition rate can be calculated as

$$G = \dot{\omega}_s M_A / \rho_A (\text{m/s or } \times 3.6 \times 10^9 \ \mu\text{m/h}), \quad (15)$$

where M_A and ρ_A are molecular weight (84 kg/kmol) and density (6.15×10^3 kg/m^3) of GaN, respectively.

6. Results and discussion

Many parameters related to the reactor geometry and mixed gas injection are important to optimal design of IVPE reactors. In this paper, we will study the effects of geometrical configurations and operating conditions on mixing process, deposition rate and deposition uniformity.

6.1. Effect of total gas flow rate on the substrate temperature

Numerical simulations have been conducted by solving the governing Eqs. (1)–(4) together with the ideal gas law and gas and surface reactions. A commercial software, CFD-ACE$^+$, from ESI has been used. The first order upwind differencing scheme (70%) blending with the third-order differencing scheme (30%) is used to discretize variables in transport equations. The Conjugate-Gradient-Squared plus Pre-conditioning solver is used to solve the algebraic equations for each dependent variable. Simulations are performed using different grid numbers for grid independent study. 165×55 grids are used for most cases presented in this paper.

A uniform and sufficient high temperature on the substrate is required to achieve high growth rate, uniform film thickness and good film quality. In the experiments, the temperature on the furnace wall is monitored using thermocouples. In situ observation of temperature achieved on the substrate surface, however, is difficult to realize. Temperature difference between the substrate surface and furnace wall, and the effect of total gas flow rate on the temperature achieved on the substrate surface will be investigated numerically. Gas species at each inlet and their flow rates used in the simulations are listed in Table 2.

The initial inlet gas conditions are tested both experimentally and numerically. The measured gallium weight reduction rate of 0.0133 SLM is used in the simulation. This flow rate corresponds to a molar ratio of Ga/$I_2 = 1.7/1$, which favors the formation of GaI in the gas phase. Temperature (1050 °C) on the heating unit and reactor pressure (200 torr) remain unchanged for all the simulations presented here. Gas phase and surface reactions are not activated in the simulation unless it is noted, since they are expected to have insignificant influence on the fluid flow and heat transfer in the reactor. Thermodynamic properties of different substances used in the simulations are listed in Table 3.

Fig. 5a–b shows the streamline and temperature distributions in the simulated system. Fig. 5a shows that a reverse flow is formed near the alumina tube wall, which means that the radial mixing of different species will be enhanced there. The gas phase reactions from GaI/NH_3 in the center part and the GaN deposition on the alumina tube wall will therefore increase, and the GaN deposition rate will decrease on the substrate. In addition, the reverse flow might be unstable in the experiments, which could be larger or smaller as the time passing. The GaN deposition quality on the substrate could therefore be worsened. Due to the above reasons, it is necessary to make sure that no big reverse flow is formed in the reactor. Fig. 5b shows the temperature distribution for the entire simulated system. It is shown that the temperature of the gas mixture

Table 2
Inlet gas conditions for the experiments

	Species	Initial volume flow rate (SLM)	Adjusted volume flow rate (SLM)
Inlet1	I_2	0.008	0.008
	H_2	0.026	0.026
	N_2	0.5	0.25
Inlet2	N_2	1.0	0.62
Inlet3	NH_3	2.0	1.0
	N_2	/	1.25

Table 3
Thermodynamic properties used in the simulations

Properties	All gases	Al_2O_3	GaN	Silica	BN
Specific heat (J/kg K)	Mix JANNAF method	900	490	710	1610
Density (kg/m^3)	Ideal gas law	3900	6150	2198	1900
Thermal conductivity (W/m k)	Mix kinetic theory	30	130	1.38	28
Dynamic viscosity (kg/m s)	Mix kinetic theory	/	/	/	/
Diffusivity	Schmidt number = 0.72	/	/	/	/
Adsorption coefficient	0	1	1	0.145	1

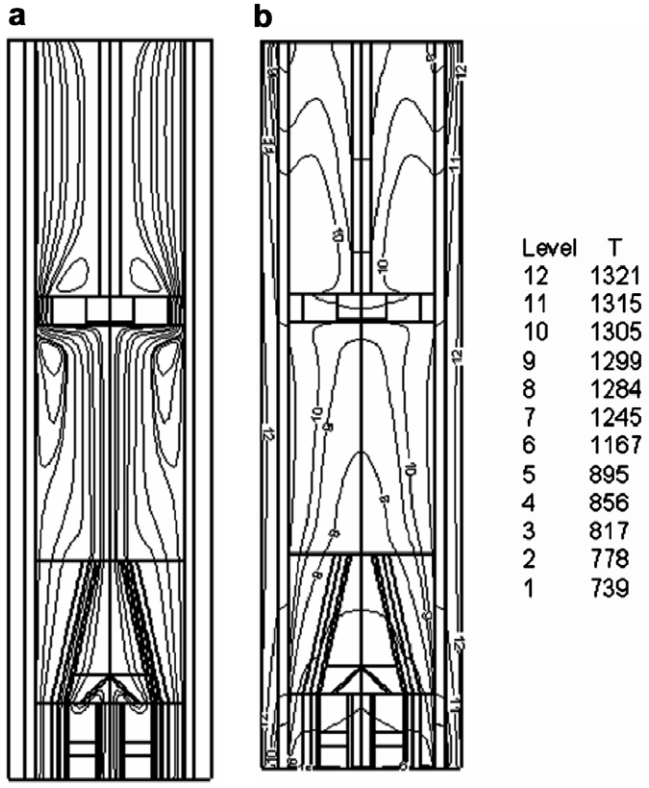

Fig. 5. Distributions of (a) streamline and (b) temperature inside the VPE reactor.

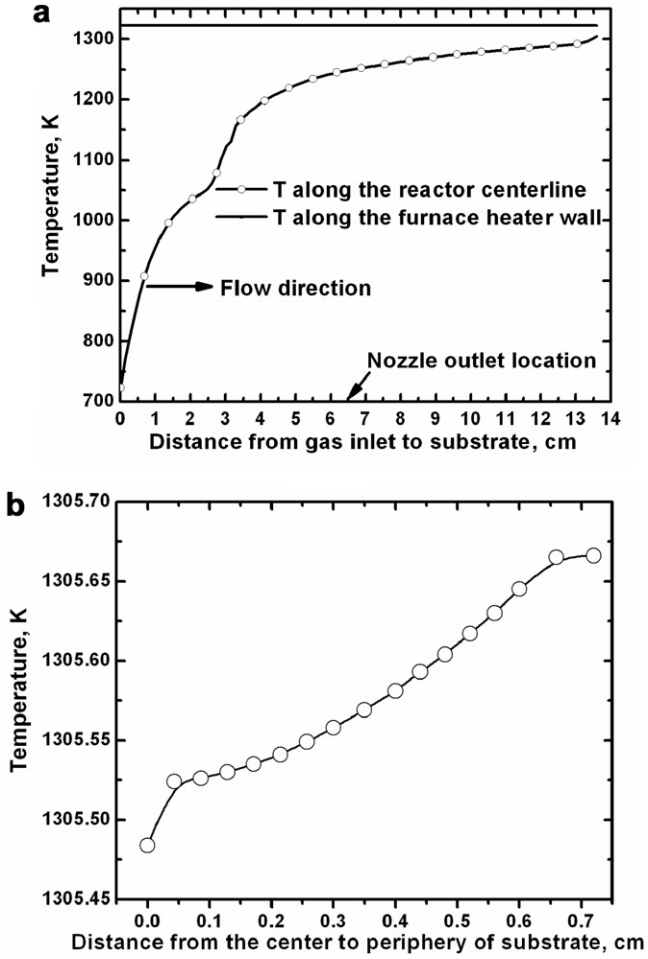

Fig. 6. Temperature distributions (a) from the gas inlet to substrate surface along the reactor centerline and furnace heater wall, and (b) from the center to periphery of the substrate surface, respectively.

will be heated up to more than 1200 K above the silica nozzle. Due to such a high-temperature, chemical deposition may occur on the surfaces of the reactor wall, substrate, and substrate holder.

The velocity ratio of NH_3 from inlet 3, shield gas N_2 from inlet 2 and carrier gas from inlet 1 are 1:11:13 at the height of the silica nozzle outlet. It can be concluded that the reverse flow is formed mainly due to a large gas velocity difference at the silica nozzle outlet. To prevent the reverse flow, an adjusted inlet gas flow rates are used in the experiment run (see Table 2). The velocity ratio under the new inlet conditions is 1:6:6. Simulations results show that the reverse flow is eliminated in this case.

Fig. 6a shows the temperature distributions from inlet to the substrate surface along the reactor centerline and along the substrate surface, based on the adjusted inlet gas conditions. It is revealed that the mixing gases can be heated to about 1250 K when it reaches the nozzle outlet and it further increases to 1300 K at the substrate area. Fig. 6b shows the temperature distribution from the periphery to the center of the substrate surface. It is found that the temperature on the substrate surface will be high at the periphery but low in the middle. Temperature difference along the substrate surface is only about 0.18 °C, and the substrate temperature is about 17 °C lower than the temperature on the furnace heater.

By reducing or increasing the flow rate at each gas inlet with the same ratio, the effect of the total flow rate on the temperature achieved on the substrate was investigated. Fig. 7a shows the averaged temperature achieved on the substrate with different total gas flow rates. It is revealed that within a flow rate range of 1–10 SLM, the substrate temperature drops from 1307 to 1283 K. Temperature non-uniformity on the substrate also changes with total flow rates. Temperature difference is defined as the highest temperature minus the smallest one on the substrate. It is revealed in Fig. 7b that a total flow rate of 3 SLM gives the lowest temperature difference, or the best uniformity, on the substrate surface. In the experiments, total flow rate is controlled at around 3 SLM.

6.2. Effect of the shield gas flow rate

The shield gas, N_2, is used to prevent Ga from mixing with NH_3 directly in the area above the silica nozzle so as to reduce the gas phase reactions from GaI and NH_3. Four cases are presented, in which the shield gas flow rates are 0.5 SLM, 0.8 SLM, 1.2 SLM and 1.5 SLM, respectively. The only reaction activated is reaction R4. Fig. 8 shows the mass fraction change of NH_3 with the shield

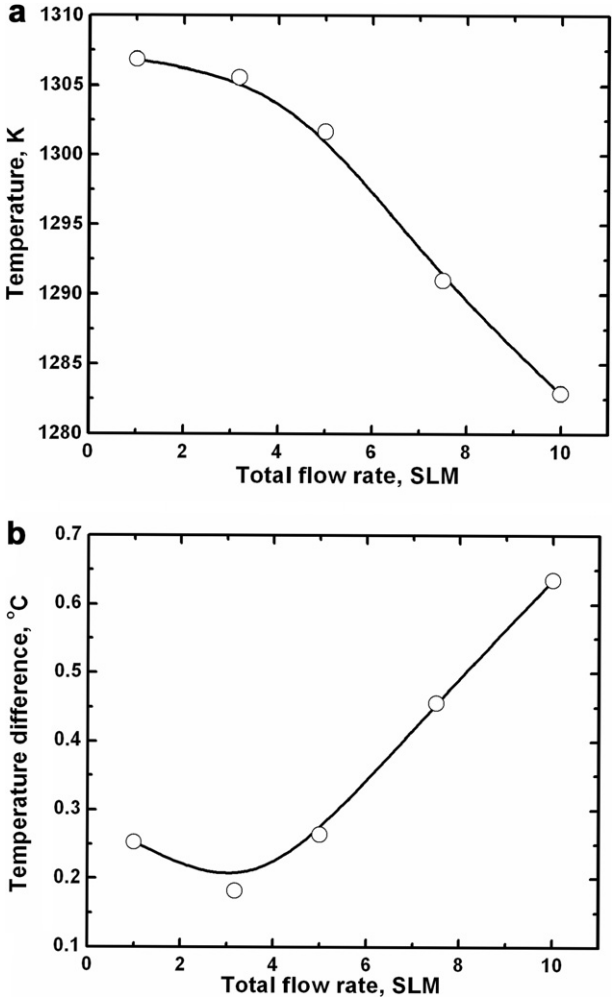

Fig. 7. Relationship of (a) averaged temperature achieved on the substrate and (b) the largest temperature difference on the substrate with the total flow rate in the growth reactor.

gas flow rate along the reactor centerline from the outlet of the silica nozzle to the substrate surface. It is revealed that at the silica nozzle outlet, NH_3 concentration is zero. It gradually increases with the distance. The concentration of NH_3 with 1.5 SLM shield gas flow rate is about half of that with 0.5 SLM shield gas flow rate along the centerline. Fig. 9a shows the averaged concentrations of GaI and NH_3 on the substrate surface. It is shown that the concentrations of GaI and NH_3 decrease as the shield gas flow rate increases. It is also observed that, the effect of shield gas flow rate on the NH_3 concentration is more significant than its effect on GaI concentration. When the shield gas flow rate increases from 0.5 SLM to 1.5 SLM, the concentrations of GaI and NH_3 drop 17% and 34%, respectively. This can be explained that the increase of the shield gas flow rate causes the increase of the N_2 concentration on substrate surface, consequently reduces the GaI and NH_3 concentrations. Furthermore, it also reduces the time allowed for NH_3 to diffuse into the center area, which further reduces the NH_3 concentration. Fig. 9b shows the V/III ratios, or the molar ratios of NH_3 and GaI, on the

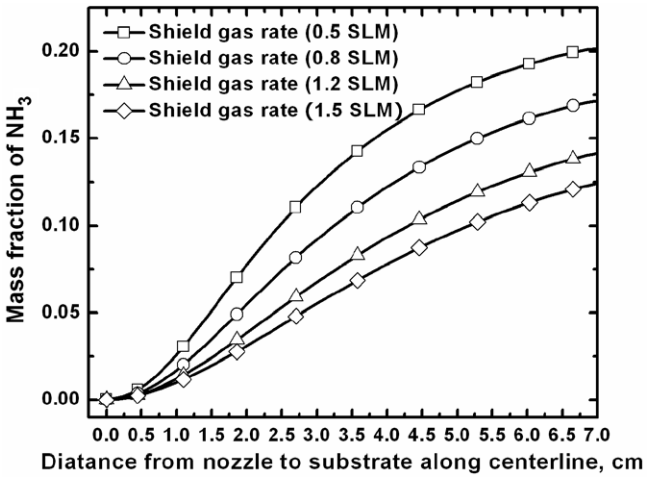

Fig. 8. Mass fraction distribution of NH_3 along the centerline from the silica nozzle to the substrate with different shield gas flow rates.

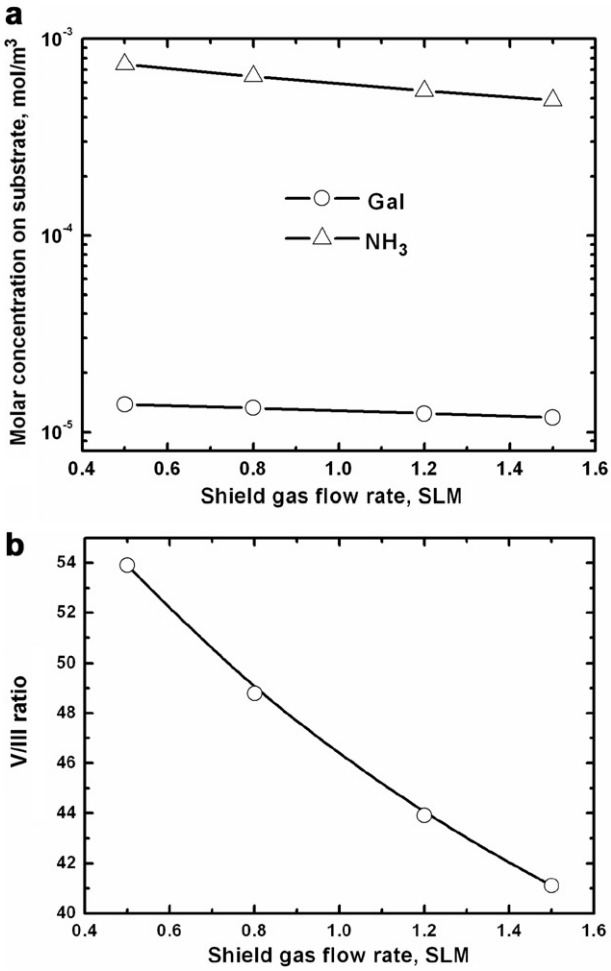

Fig. 9. Relationship of (a) averaged concentrations of GaI and NH_3 on the substrate and (b) the V/III ratios achieved on the substrate with the shield gas flow rate.

substrate surface. The NH_3 concentration reduces due to the increase of the shield gas flow rate, consequently the V/III ratio reduces with the shield gas flow rate.

Experiments were conducted to study the shield gas flow rate on the GaN deposition rate. The shield gas flow rates of 0.62 SLM and 1.0 SLM are used in the experiments, respectively. The flow rate of 0.62 SLM corresponds to the velocity ratio of 1:1 between the shield gas and rest gases at the outlet of the silica nozzle. The GaN deposition rates at different iodine concentrations and shield gas flow rates have been reported by Mecouch [30] and they are shown in Fig. 10. It is seen that the shield gas flow rate of 0.62 SLM produces higher GaN growth rate under different iodine concentrations in the source bubbler. A shield gas flow rate of 0.62 SLM is therefore used in the subsequent experiments. Fig. 11a and b shows the mass fraction distributions of GaI and NH_3 in the growth reactor. It is revealed in Fig. 11a that the gas phase reaction between Ga and I_2 takes place mainly inside the inner silica nozzle. Since the gas flow in the reactor is laminar (see Fig. 11b), the transport of NH_3 into the center area of the reactor is due to mass diffusion.

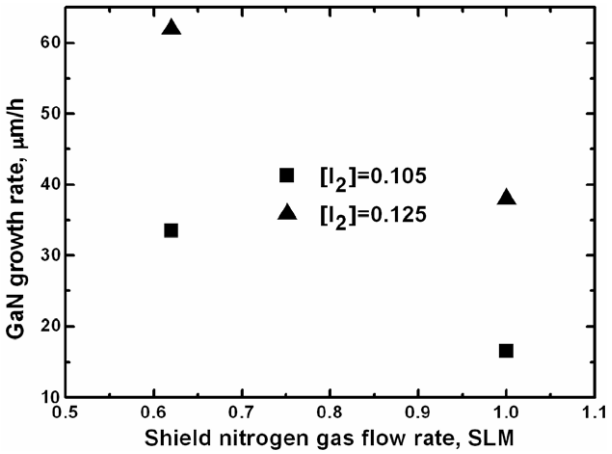

Fig. 10. Change of the GaN deposition rate with the shield gas flow rate under different iodine concentrations.

The mass fraction, Y_i, the molar concentration, C_i, and the partial pressure, P_i, of species i on the substrate are listed in Table 4 when a shield gas flow rate of 0.62 SLM is used in the simulations.

The results show that the partial pressure of Ga is close to zero, and the achieved partial pressure of GaI is around 1 torr on the substrate at a reactor pressure of 200 torr.

6.3. Effect of silica nozzle angle

The GaN growth rate is directly proportional to the partial pressure of GaI achieved on the substrate. A silica nozzle is thus used in the experiments to force more GaI to the substrate area. This will also help preventing ammonia from diffusing towards the gallium source area because ammonia reacts with Ga directly on the liquid gallium surface to form polycrystalline GaN through the reaction listed below:

$$2Ga(g) + 2NH_3(g) \rightarrow 2GaN(s) + 3H_2(g). \quad (R23)$$

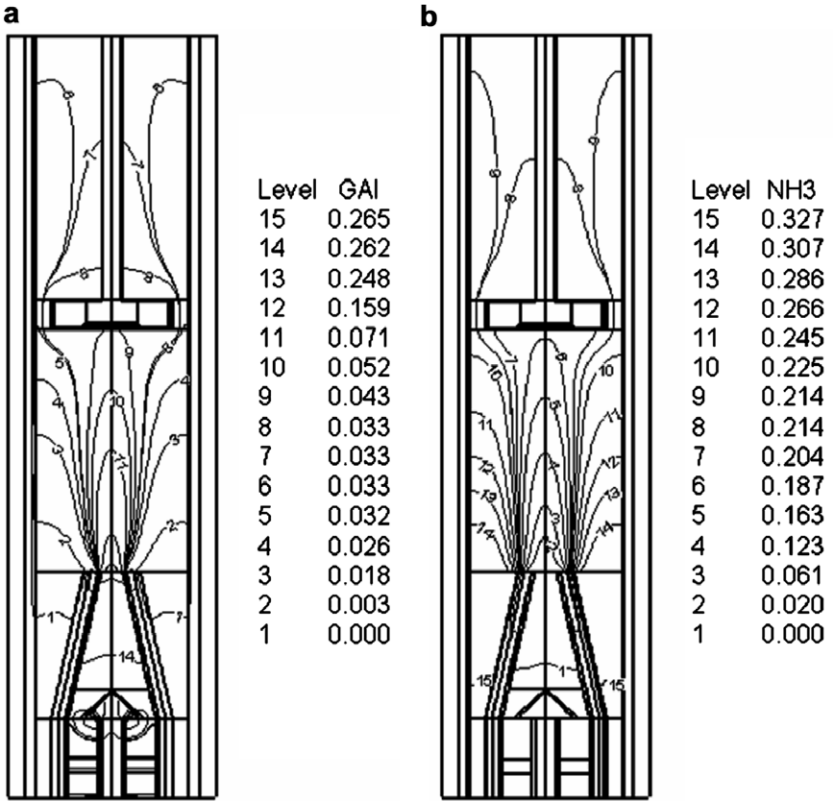

Fig. 11. Mass fraction distributions of (a) GaI and (b) NH_3 inside the VPE reactor.

Table 4
Species concentrations on the substrate

	Ga	GaI	H_2	I_2	N_2	NH_3
Y_i	2.4E−06	0.042575	0.000855	0.005494	0.760977	0.190096
C_i (kmol/m^3)	2.16E−09	1.36E−05	2.69E−05	1.36E−06	1.71E−03	7.02E−04
P_i (torr)	1.76E−04	1.11E+00	2.19E+00	1.11E−01	1.39E+02	5.73E+01

This reaction (R23) could terminate the transport of gallium and stop the GaN growth on the substrate.

Design of silica nozzle angle, θ (see Fig. 1a), is very important. To test the effect of nozzle angle on concentration distributions of NH_3 and GaI between the outlet of silica nozzle and substrate surface, four cases are simulated in which θ is selected as 77°, 81°, 86° and 90°. Fig. 12 shows the mass fraction distribution of NH_3 along the reactor centerline from the silica nozzle outlet to the substrate surface. It is found that at the silica nozzle outlet, the NH_3 concentration for the cases with the angle smaller than 81° is close to 0. For angles larger than 81°, the achieved ammonia mass fraction is up to 0.03 at the outlet of the inner silica nozzle, which means that ammonia may diffuse into the inner silica tube. It is also seen that a small angle, such as 77°, can significantly reduce the NH_3 concentration in the area above the silica nozzle. The blocking effect, however, reduces as the mixing gas approaching the substrate, so the concentration of NH_3 on the substrate is maintained at a proper level even with a small nozzle angle. Fig. 13a shows the average molar concentrations of GaI and NH_3 on the substrate surface. The concentration of NH_3 increases with the nozzle angle, while that of GaI decreases with the nozzle angle. It is shown in Fig. 13b that the V/III ratio on the substrate surface increases with the nozzle angle.

The silica nozzle angle used in the experiment is 77°.This design of silica nozzle can reduce the NH_3 concentration in the area above the silica nozzle outlet significantly. Diffusion of NH_3 into the inner silica nozzle is prevented. The GaI concentration on the substrate can be increased by about 10% compared with a silica nozzle angle of 90°.

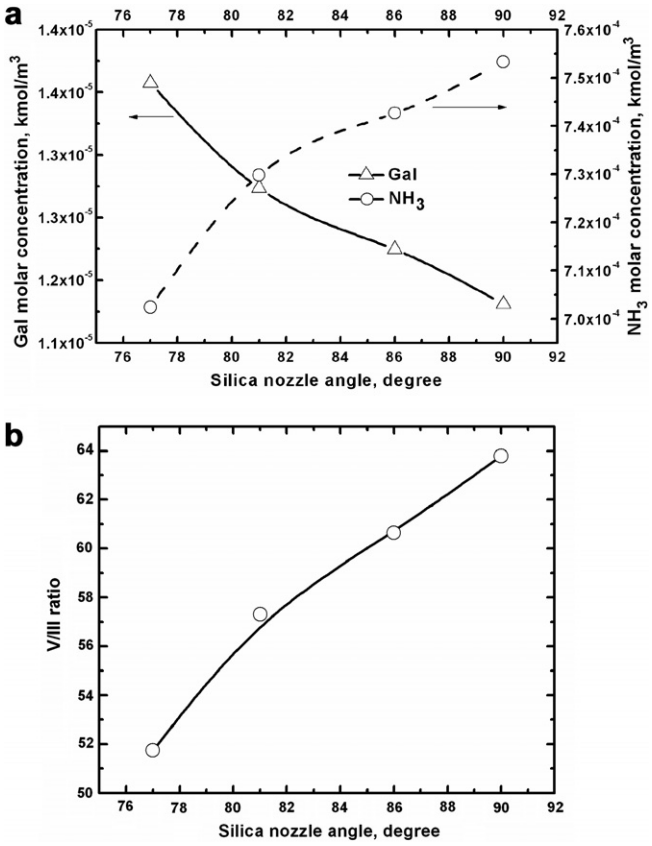

Fig. 13. Relationship of (a) averaged concentrations of GaI and NH_3 on the substrate and (b) the V/III ratio achieved on the substrate with different silica nozzle angles.

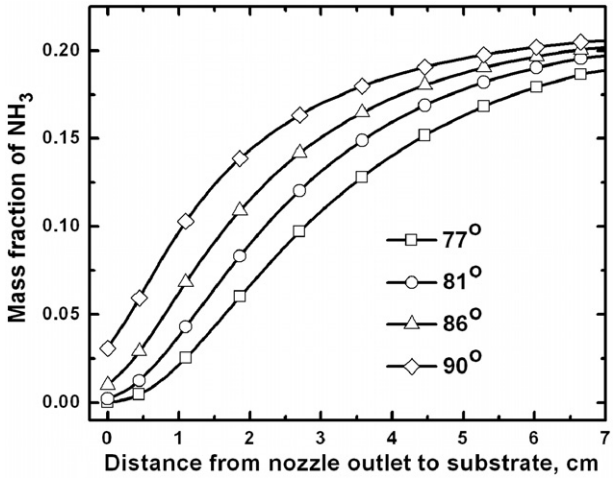

Fig. 12. Mass fraction distribution of NH_3 along the centerline from the silica nozzle to the substrate under different silica nozzle angles.

6.4. Effect of the substrate-nozzle distance

The substrate-nozzle distance is one of the key parameters that affect the GaN growth rate and deposition quality. It controls the length and time allowed for different gases to mix with each other. A proper substrate-nozzle distance corresponds to a suitable V/III ratio above the substrate for fast and uniform GaN growth. The simulated substrate-nozzle distance ranges from 6.35 to 17.8 cm. Fig. 14a shows the molar concentrations of GaI and NH_3 as a function of the substrate-nozzle distance. The concentration of GaI decreases with the substrate-nozzle distance until the mixing is completed at the substrate-nozzle distance around 13.0 cm. The error bar in Fig. 14a indicates the GaI concentration variation across the substrate

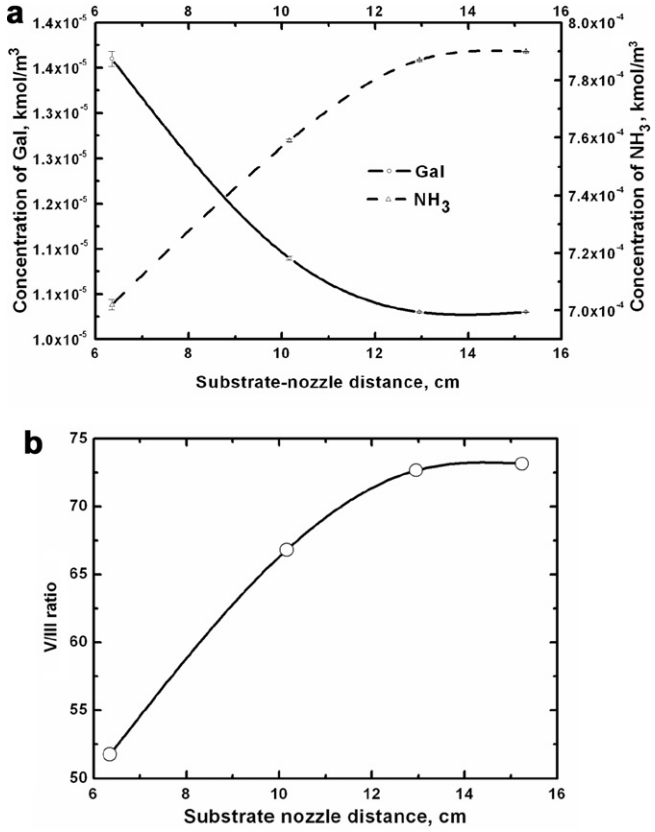

Fig. 14. (a) Averaged molar concentrations of GaI and NH_3 and (b) the V/III ratio achieved on the substrate under different substrate-nozzle distances.

surface. It is found that even for a small substrate-nozzle distance of 6.35 cm, variation of GaI concentration on the substrate surface is small (around 0.6%), which means that the species uniformity is not a problem. The concentration of NH_3 increases with the distance since more time is available for ammonia to diffuse into the center area of the reactor. Variation of V/III ratio with the substrate-nozzle distance is shown in Fig. 14b. It is found that when the substrate-nozzle distance is less than 13.0 cm, a substrate-nozzle distance increase of 2.5 cm corresponds to a V/III ratio increase of 10.

It is concluded that a complete mixing of different species needs a substrate-nozzle distance larger than 13.0 cm. Species concentration across the substrate surface is, however, fairly uniform even with a small substrate-nozzle distance such as 6.35 cm. In the experiments, a uniform GaN deposition with a high growth rate is preferred. The substrate-nozzle distance of 6.35 cm is used due to that species concentrations are uniform across the substrate surface and a high GaI concentration of 1.4×10^{-5} kmol/m^3 can be achieved. The V/III ratio in this case will be about 50. For the growth of GaN from GaI_{1-3}/NH_3 or $GaCl_{1-3}/NH_3$, the concentration of NH_3 is maintained at a high value on the substrate since it is easy to realize and it will result in a proper super-saturation as the driving force for the surface deposition. For the current GaN vapor growth system, the V/III ratio is kept above 50 for most experimental runs.

6.5. Deposition test

Combined with the experimental data, the GaN deposition rate at a constant growth temperature of 1050 °C is tested numerically, while the flow rates at the inlets are changed to obtain different reactant concentrations and V/III ratios on the substrate. More importantly, simulations are performed to test the surface reaction path of GaN growth and the contribution of different reactions to the final GaN growth rate.

The energetically preferred surface reactions on the substrate for the GaN deposition have been obtained early. Reaction (R18) is first used as the overall surface reaction step on the substrate in numerical simulations. Fig. 15 shows the experimental data of the GaN deposition rate at different ammonia flow rates and iodine vapor fractions. The highest growth rate achieved is 65 μm/h. It is revealed that the GaN growth rate is independent of the NH_3 flow rate but related strongly to the GaI concentration.

Experiments have been conducted to examine the effects of V/III ratio on the GaN deposition rate. The V/III ratio is changed through maintaining the NH_3 flow rate at 1 SLM while changing I_2 concentration in the source. Using the same operating conditions as experiment, simulations are conducted in which reaction (R18) is used as a boundary condition. The surface reaction rate coefficient, δA_p, and the concentration dependency of GaI, α, are determined by fitting the simulation results with the experimental data. Fig. 16a shows the GaN deposition rate with the V/III ratio.

The surface reaction rate of reaction (R18) used to obtain the numerical results in Fig. 16a is determined by the following equation:

$$\dot{w} = 6.5 \times 10^9 \mathrm{Exp}(-12390/T)[\mathrm{GaI}]^{2.2}. \quad (16)$$

It is concluded that when one overall surface reaction step is used to predict the GaN deposition rate, the reaction rate

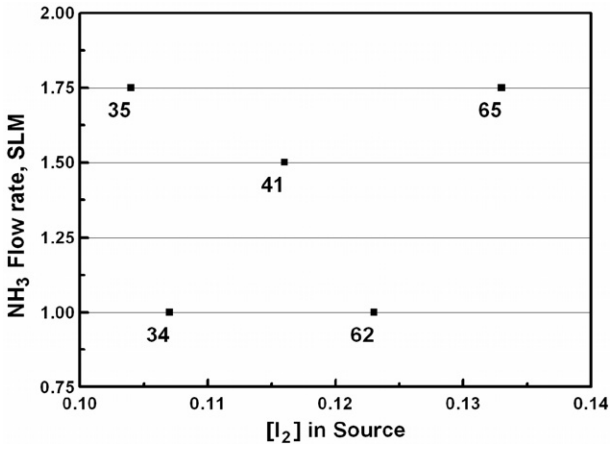

Fig. 15. Effects of changing ammonia flow rate and iodine vapor fraction in the source on the GaN deposition rate.

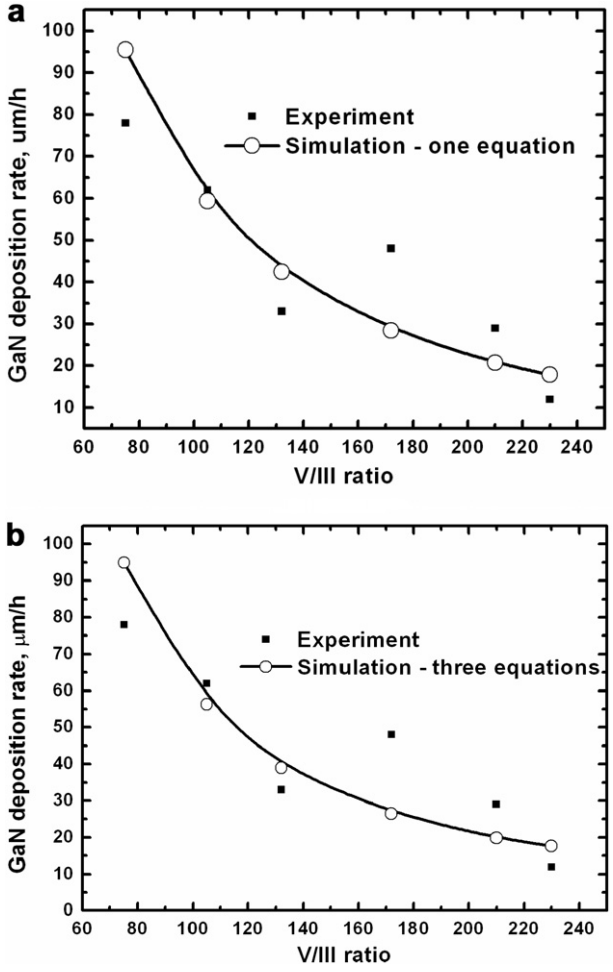

Fig. 16. GaN deposition rate as a function of the V/III ratio for (a) one surface reaction and (b) three surface reactions.

coefficient is 6.5×10^9 and the GaI concentration dependency is 2.2.

When reactions (R18)–(R20) are all used in the simulation, the reaction rate coefficient of each reaction is determined by matching the simulation results with the experimental data. Fig. 16b shows the GaN deposition rate calculated using all of three surface reactions and the deposition rates from the experiment. The surface reactions and their reaction rates used in this paper are summarized in Table 5.

The calculated GaN deposition rate due to reactions (R18) and (R19) is presented in Table 6. Since GaI is considered as the only medium for Ga source transport, the contribution of reaction (R20) to the deposition rate is found to be less than 0.1% for all cases and is therefore not listed in Table 6. In the experiment, the contribution of reaction (R20) to the GaN deposition rate might be larger. It is, however, not expected to be as significant as reactions (R18) and (R19). It is revealed that, the contribution of reaction (R18) to total GaN deposition rate increases with the V/III ratio, while for reaction (R19) it decreases with the V/III ratio.

Table 6
GaN deposition rate and rate contribution from reactions R18 and R19

V/III ratio	GaN deposition rate (μm/h)		Growth rate contribution (%)	
	Reaction (R18)	Reaction (R19)	Reaction (R18)	Reaction (R19)
75	21.80	73.10	22.97	77.03
105	17.62	38.61	31.33	68.67
132	15.04	24.01	38.52	61.48
172	12.54	13.89	47.41	52.59
210	10.86	9.03	54.60	45.40
230	10.16	7.40	57.86	42.14

The super-saturation of GaN growth on the substrate can be calculated once the partial pressure of each species is obtained. Fig. 17 shows the calculation results of the super-saturation with different reactor temperatures. The super-saturation is around 5. It is typical for an epitaxy growth system which needs a relatively low super-saturation to prevent the reactant partial pressures deviating excessively from the equilibrium values. The super-saturation reduces with the temperature slightly, which means that the GaN deposition is diffusion controlled under the current operating conditions.

Table 7 summarizes the sticking probability of the reacting species deduced from various simulations. The calculated sticking probabilities of the order of 10^{-3}–10^{-6} are reasonable for saturated compound. The sticking probability of species i, S_i, is defined by the following equation:

$$S_i = f(\theta^s)_i \cdot \exp[-E_{ai}(\theta^s)/RT] = R_i/F_i, \quad (17)$$

where $f(\theta^s)_i$ is the function of the existing surface coverage of adsorbed species i, θ^s is the Langmuir definition of surface coverage of certain species, or the fraction of sites which are occupied on the substrate surface, E_{ai} is the activation energy for adsorption of species i, R_i (kmol/m^2 s) is the rate of adsorption of species i chemically, and $F_i = P_i^w/(2\pi RTM_i)^{1/2}$ (kmol/m^2 s) is the incident flux rate of species i onto the substrate.

It is observed that the sticking probability decreases with the increase of V/III ratio. This indicates that when the I_2 concentration decreases in the source, the species reaction rate decreases more significantly compared with its incident flux onto the substrate. The sticking probability

Table 5
Surface reaction rates obtained by matching simulation result with experimental data

Reaction	Rate expression (kmol/m^2 s)
(R18) $GaI(g) + NH_3(g) \Leftrightarrow GaN(s) + HI(g) + H_2(g)$	$0.07\exp(-12390/T)[GaI]$
(R19) $3GaI(g) + 2NH_3(g) \Leftrightarrow 2GaN(s) + GaI_3(g) + 3H_2(g)$	$5.88E+09\exp(-13630/T)[GaI]^3$
(R20) $GaI_3(g) + NH_3(g) \Leftrightarrow GaN(s) + 3HI(g)$	$0.36\exp(-14000/T)[GaI_3]$

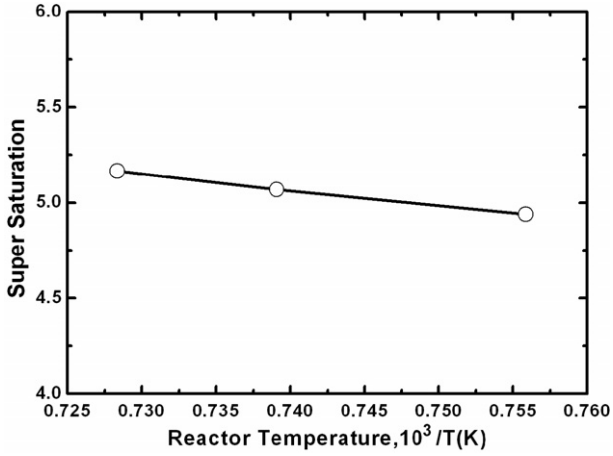

Fig. 17. Super-saturation of GaN growth under different reactor temperature.

Table 7
Sticking probability of reactant i with different V/III ratios

V/III ratio	Sticking probability		
	GaI ($\times 10^3$)	NH_3 ($\times 10^6$)	GaI_3 ($\times 10^3$)
75	2.66	6.50	4.15
105	2.07	4.10	3.12
132	1.75	3.02	2.69
172	1.43	2.08	2.07
210	1.22	1.55	1.86
230	1.13	1.38	1.77

of ammonia is three orders of magnitude smaller than GaI and GaI_3, since ammonia concentration is kept much higher than GaI on the substrate.

To determine the activation energy for adsorption of species i, it is assumed that the sticking probability is directly proportional to the concentration of vacant surface sites, i.e. $(1-\theta^s)$. So $f(\theta^s)$ is proportional to $(1-\theta^s)$. This assumption is a reasonable first approximation for non-dissociative adsorption. The activation energy of adsorption is

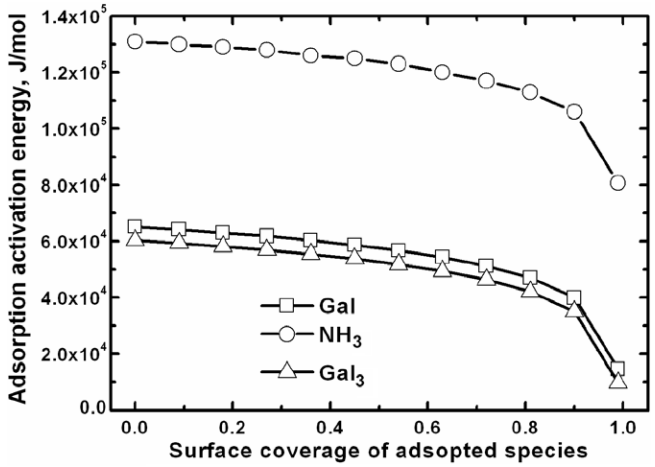

Fig. 18. Activation energy of adsorption with a surface coverage range of 0–0.99.

assumed to be independent of the surface coverage. So the sticking probability can be revised as follows:

$$S_i = (1-\theta^s)\cdot \exp(-E_{ai}/RT). \quad (18)$$

Fig. 18 shows the calculated activation energy of adsorption for three species with a surface coverage range of 0–0.99. The activation energy drops as the surface coverage increases. The averaged activation energies of adsorption for GaI, NH_3 and GaI_3 by calculation are 5.72×10^4 J/mol, 1.24×10^5 J/mol and 5.28×10^4 J/mol, respectively.

7. Conclusions

Numerical and experimental studies have been performed to study heat and mass transfer in a vertical hot-wall gallium nitride epitaxy growth system. The study of gas phase reactions shows that instead of thermodynamic indication of GaI_3 as the main transport species for the gallium source, GaI is kinetically favored due to the fact that reactions between liquid gallium and I_2 gas is far from equilibrium on the gallium surface. The results obtained from the surface reaction analysis show that the GaN deposition rate is limited by the surface adsorption of GaI. It is, however, independent of the ammonia concentration on the substrate. The operating and geometrical conditions for fast and uniform GaN growth have been optimized numerically and experimentally. The optimum total flow rate for a sufficient high-temperature with the best uniformity on the substrate surface has been identified to be 3 SLM. The preferred silica nozzle angle, shield gas flow rate, and substrate-nozzle distance are determined as 77°, 0.62 SLM and 6.35 cm, respectively.

The super-saturation has been calculated to be around 5, and the fact that the value of super-saturation does not change much with the substrate temperature reveals that the growth rate is diffusion controlled. The kinetic data for surface reactions are obtained by fitting the experimental data with the simulation results. The contribution of the three surface reactions to the GaN deposition rate has been evaluated and the reaction (R20) is found to account for less than 0.1% of the total deposition rate. Reactions (R18) and (R19) are both important under the V/III ratio range of 75–230. The sticking probabilities of reactants are calculated and it is found that the sticking probabilities for GaI and GaI_3 are around 10^{-3}. The sticking probability of NH_3 is about 3 orders of magnitude lower than GaI and GaI_3. The adsorption energies of the species on the substrate surface have been evaluated and the results reveal that the sticking activation energies for GaI, NH_3, and GaI_3 are 5.72×10^4 J/mol, 1.74×10^5 J/mol and 5.28×10^4 J/mol, respectively.

Acknowledgements

This work is supported by the DoD Multidisciplinary University Research Initiative (MURI) program adminis-

tered by the Office of Naval Research under Grant N00014-01-1-0716.

References

[1] S. Nakamura, III–V nitride based light-emitting devices, Solid State Commun. 102 (2–3) (1997) 237.
[2] S.C. Jain, M. Willander, J. Narayan, R. Van Overstraeten, III-nitrides: growth, characterization, and properties, J. Appl. Phys. 87 (3) (2000) 965–1006.
[3] G. Kamler, J. Zachara, S. Podsiadlo, L. Adamowicz, W. Gebicki, Bulk GaN single-crystals growth, J. Crystal Growth 212 (1–2) (2000) 39–48.
[4] B. Wu, R.H. Ma, H. Zhang, Epitaxy growth kinetics of GaN films, J. Crystal Growth 250 (1–2) (2003) 14–21.
[5] R.J. Molnar, W. Gotz, L.T. Romano, N.M. Johnson, Growth of gallium nitride by hydride vapor-phase epitaxy, J. Crystal Growth 178 (1–2) (1997) 147–156.
[6] T. Paskova, E.M. Goldys, B. Monemar, Hydride vapor-phase epitaxy growth and cathodoluminescence characterisation of thick GaN films, J. Crystal Growth 203 (1–2) (1999) 1–11.
[7] M. Suscavage, L. Bouthillette, D. Bliss, S.Q. Wang, C. Sung, New iodide method for growth of GaN, Phys. Status Solidi A – Appl. Res. 188 (2) (2001) 477–480.
[8] V. Tassev, D. Bliss, M. Suscavage, Q.S. Paduano, S.Q. Wang, L. Bouthillette, Iodine vapor phase growth of GaN: dependence of epitaxial growth rate on process parameters, J. Crystal Growth 235 (1–4) (2002) 140–148.
[9] N. Kaluza, R. Steins, H. Hardtdegen, H. Lueth, MOVPE GaN growth: determination of activation energy using in situ reflectometry, J. Crystal Growth 272 (1–4) (2004) 100–105.
[10] K. Harafuji, Gas-phase and surface reactions in a horizontal reactor for GaN MOVPE growth, Phys. Status Solidi A – Appl. Res. 188 (2) (2001) 635–639.
[11] S.A. Safvi, N.R. Perkins, M.N. Horton, R. Matyi, T.F. Kuech, Effect of reactor geometry and growth parameters on the uniformity and material properties of GaN/sapphire grown by hydride vapor-phase epitaxy, J. Crystal Growth 182 (3–4) (1997) 233–240.
[12] G. Attolini, S. Carra, F. Di Muzio, R. Fornari, M. Masi, C. Pelosi, A vertical reactor for deposition of gallium nitride, Mater. Chem. Phys. 66 (2–3) (2000) 213–218.
[13] C.E.C. Dam, A.P. Grzegorczyk, P.R. Hageman, R. Dorsman, C.R. Kleijn, P.K. Larsen, The effect of HVPE reactor geometry on GaN growth rate – experiments versus simulations, J. Crystal Growth 271 (1–2) (2004) 192–199.
[14] F.M. White, Viscous Fluid Flow, second ed., McGraw-Hill, New York, 1991.
[15] T.K. Sherwood, R.J. Pigford, C.R. Wilke, Mass Transfer, first ed., McGraw-Hill, New York, 1975.
[16] L.C. Burmeister, Convective Heat Transfer, second ed., Wiley, New York, 1993.
[17] M.F. Modest, Radiative Heat Transfer, McGraw-Hill, New York, 1993.
[18] R. Cadoret, Growth mechanisms of (0 0 1)GaN substrates in the hydride vapour-phase method: surface diffusion, spiral growth, H-2 and GaCl3 mechanisms, J. Crystal Growth 205 (1–2) (1999) 123–135.
[19] D.F. Davidson, K. Kohsehoinghaus, A.Y. Chang, R.K. Hanson, A pyrolysis mechanism for ammonia, Int. J. Chem. Kinet. 22 (5) (1990) 513–535.
[20] D.R. Stull, Vapor pressure of pure substances – organic compounds, Ind. Eng. Chem. 39 (4) (1947) 517–540.
[21] O. Knacke, O. Kubaschewski, K. Hesselmann (Eds.), Thermochemical Properties of Inorganic Substances I, second ed., Springer-Verlag, Berlin, 1991.
[22] I. Barin, Thermochemical Data of Pure Substances, VCH, Weinheim, 1989.
[23] Thermodynamics Research Center, NIST Boulder Laboratories, M. Frenkel director, "Thermodynamics Source Database" in NIST Chemistry WebBook, NIST Standard Reference Database Number 69, P.J. Linstrom, W.G. Mallard (Eds.), March 2003, National Institute of Standards and Technology, Gaithersburg MD, 20899, <http://webbook.nist.gov>.
[24] R.F. Rolsten, Iodide Metals and Metal Iodides, Hogh Wiley & Sons, New York, 1961.
[25] W.J. Mecouch, Preparation and characterization of thin, atomically clean GaN(0001) and AlN(0001) films and the deposition of thick gan films via iodine vapor phase growth, PH.D thesis, Materials Science and Engineering Department, North Carolina State University, 2005.
[26] A. Shintani, S. Minagawa, Kinetics of epitaxial-growth of GaN using Ga, HCl and NH_3, J. Crystal Growth 22 (1) (1974) 1–5.
[27] D.W. Shaw, Influence of substrate temperature on gas epitaxial deposition rates, J. Electrochem. Soc. 115 (4) (1968) 405.
[28] A. Dollet, Y. Casaux, G. Chaix, C. Dupuy, Chemical vapor deposition of polycrystalline A1N films from AlCl3–NH3 mixtures. Analysis and modeling of transport phenomena, Thin Solid Films 406 (1-2) (2002) 1–16.
[29] D. Cai, L.L. Zheng, H. Zhang, V.L. Tassev, D.F. Bliss, Modeling of aluminum nitride growth by halide vapor transport epitaxy method, J. Crystal Growth 276 (1–2) (2005) 182–193.
[30] W.J. Mecouch, B.J. Rodriguez, Z.J. Reitmeier, J.S. Park, R.F. Davis, Z. Sitar, Initial stages of growth of gallium nitride via iodine vapor phase epitaxy, in: Materials Research Society Symposium Proceeding, vol. 831, 2005, p. E3.23.1.